Journal of Emerging and Selected Topics in Power Electronics,Vol. 3, No. 1, pp. 252 - 260, March 2015

Transmission Line Resistance Compression Networks and Applications to Wireless Power Transfer

Taylor W. Barton, *Member, IEEE,* Joshua M. Gordonson, and David J. Perreault, *Fellow, IEEE*

***Abstract*—Microwave-to-dc rectification is valuable in many applications including rf energy recovery, dc-dc conversion, and wireless power transfer. In such applications, it is desired for the microwave rectifier system to provide a constant rf input impedance. Consequently, variation in rectifier input impedance over varying incident power levels can hurt system performance. To address this challenge, we introduce multi-way transmission-line resistance compression networks (TLRCNs) for maintaining near-constant input impedance in rf-to-dc rectifier systems. A development of TLRCNs is presented, along with their application to rf-to-dc conversion and wireless power transfer. We derive analytical expressions for the behavior of TLRCNs, and describe two design methodologies applicable to both single and multi-stage implementations. A 2.45-GHz 4-way TLRCN network is implemented and applied to create a 4-Watt resistance-compressed rectifier system that has narrow-range resistive input characteristics over a 10-dB power range. It is demonstrated to improve the impedance match to mostly-resistive but variable input impedance class-E rectifiers over a 10-dB power range. The resulting TLRCN plus rectifier system has >50% rf-to-dc conversion efficiency over a >10-dB input power range at 2.45 GHz (peak efficiency 70%), and SWR <1.1 over a 7.7-dB range, despite a non-negligible reactive component in the rectifier loads.**

***Index Terms*—transmission lines, impedance matching, resonant rectifiers, rectennas, wireless power transfer**

I. Introduction

IN many applications it is desirable to implement microwave rectification to capture rf energy and convert it to dc power. Such applications include energy recovery from terminations such as isolation ports in rf power amplifier systems [1], dc-dc conversion [2]–[4], and wireless power transfer [5]–[16]. In each case, it is desirable for the rf impedance at the rectifier input to appear constant and resistive across a wide range of incident power levels (e.g., to maintain impedance matching or isolation, or to minimize reflected power, etc.). In this paper, we focus on a means for maintaining near-constant input impedance in microwave-to-dc rectifier systems.

Wireless power transmission systems in particular can benefit from improvements in the match between the antenna and rectifier. Far-field powering systems, whether directive power beaming [5]–[12], [16], or low-power far-field harvesting [13]–[15], use a rectenna consisting of an antenna, rectifier, and power management circuit to convert incident rf power into stored dc energy as in the generalized block diagram in Fig. 1. In order to maximize the rectenna (rectifier + antenna) efficiency, it is desirable to provide a conjugate match between the antenna impedance and that at the input to the rectifier. However, for different incident power levels, the input impedance to an rf rectifier typically varies [1], [2], [11], [17]–[20]. The nonlinear rectifier impedance is commonly characterized at a specified incident power level and the antenna characteristic impedance and/or matching network is designed to optimize power transfer at this operating point [11]–[13], [17]. Alternatively, multiple rectifiers optimized at different incident power levels can be connected in parallel to extend the operating range of the rectenna [21]. In applications where the incident rf power density has variation over relatively slow timescales, an optimum load or maximum power point tracking (MPPT) approach can be used to optimize efficiency over a wide operating range [22]–[25]. In this approach, the rectifier is loaded with a power converter stage, with a control loop adaptively adjusting the rectifier output voltage to maximize the energy capture. In applications where the input power is modulated or varies quickly, however, the MPPT approach is limited by the narrow bandwidth for adapting the rectifier voltage inherent to the closed-loop nature of this approach. Furthermore, this approach introduces additional complexity, size, and loss of the added converter stage. It is therefore ideally desirable to develop a solution in which rf impedance at the rectifier input appears constant and resistive across a wide range of power levels and for rapid variations in incident power.

Variations in the incident rf power density are particularly common in tracking applications in which either the transmitter or receiver is moving. Examples of such high-power wireless power transfer applications include the coupling of a solar-powered satellite (SPS) with microwave transfer to either Earth or other satellites [5]–[7], as a means to provide increased energy to a transfer vehicle in low-earth orbit to augment propulsion [8], and for the wireless powering of low-altitude airborne vehicles including helicopters [9]. Recently, there has been interest in using high-power microwave power transmission to high altitude platforms (HAPs) acting as communications basestations for both powering and station keeping [26]–[29]. Because these HAPs experience long periods of shadowing (e.g., longer than geostationary earth orbit satellites), they otherwise require carrying heavy batteries, making them ideal candidates for augmented power

Manuscript received January 28, 2014; revised April 5, 2014; accepted April 9, 2014.
The authors are with the Massachusetts Institute of Technology, Cambridge, MA, 02139 USA (e-mail: tbarton@mit.edu; jomg@mit.edu; djperrea@mit.edu).

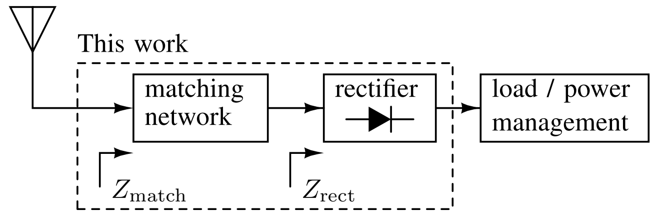

Fig. 1. Generalized rectenna block diagram. This work focuses on improving the match between the antenna and rectifier input by replacing the matching network with a transmission-line based resistance compression network that maintains near-constant input impedance over a wide range of incident power levels.

from the ground. In these and related applications, required incident power levels may be significantly higher than the power-handling capability of individual rectifier stages, an effect exacerbated at microwave frequencies where power handling of devices is limited. In order to meet the high powers (100's to 1000's of W) required, it is therefore necessary in such applications to use an array of receiving elements, with balanced power distribution of the input power among a large number of rectifiers.

In this work, we explore the use of transmission-line resistance compression networks (TLRCNs) to interface between an rf input and a plurality of rectifiers, minimizing the effective input impedance variation and acting as an impedance transformation stage. Although we focus on a four-way implementation, in which input power (incident on a single antenna) is evenly divided among four rectifiers, the technique can easily extend to eight-way or higher-order implementations. Resistance compression networks (RCNs) are a special class of matching network that provide reduced impedance variation at the rf input as compared to the rectifier inputs. The transmission-line approach in this work is related to one using discrete elements, an idea that has been applied to resonant dc-dc converters [3], [4], [18], [30] and in isolation-port energy recovery in outphasing systems [1]. At microwave frequencies, however, discrete RCN networks have severe limitations relating to the component non-idealities and interconnect parasitics and pose significant manufacturing difficulties (similar to issues arising with lumped power combiners [31], [32]). Recently, initial work has explored the use of resistance compression networks which incorporate transmission-line sections and are suitable for microwave frequencies [33]–[37]. A two-way TLRCN based on a pair of transmission-line sections (asymmetric about a 90-degree base length) was described in [35], [36] for energy recovery in outphasing power amplifiers. Although these works recognize the potential for compressive behavior in transmission-line networks using half-wavelength base lengths, they lack a complete design methodology (including selection of design values and consideration of alternative transmission line base lengths), and do not achieve sufficient resistance compression required for isolation or rectenna applications requiring low return loss.

In this paper we develop both theory and design methodologies for TLRCNs and their application to microwave rectification, following on the authors' related conference paper [37]. Balanced splitting of the input power to multiple loads along with small variation in driving-point impedance is achieved through a network consisting only of transmission line segments. We first show that additional base lengths (in addition to 90 degrees) can be employed for TLRCNs, enabling more flexible system design while minimizing losses. Second, we show that as with the related discrete-component resistance compression networks of [18], [38], multi-stage (or "multi-way") TLRCNs can be realized that achieve smaller input resistance variations than single-stage designs. In addition to providing improved input impedance characteristics, an advantage of such multi-way TLRCNs is that they distribute the input power equally among several rectifiers, which is particularly advantageous at frequencies where power-handling of rectifiers is limited and multiple devices must be used. Compared to other techniques including MPPT approaches, the TLRCN has further advantages including high bandwidth and lack of a need for a subsequent controlled converter stage. Furthermore, we introduce two design methodologies for TLRCNs. These methods enable one to select the transmission line base lengths and characteristic impedances for two-way and multi-way designs as in Fig. 2.

In order to demonstrate the TLRCN for high-power wireless power transfer applications, we have developed a prototype system operating in the 2.45 GHz ISM band. A class-E resonant rectifier providing ideally near-resistive but variable input impedance is demonstrated along with a TLRCN to significantly improve efficiency due to impedance matching between the RF source and rectifier. Scaling the 4-W demonstration to higher powers can be achieved by a straightforward array of like elements with the dc outputs connected in parallel. Because the focus of this demonstration is on the impedance match, we characterize the efficiency by directly connecting to a generator including mismatch loss but without an antenna. Wireless power transfer is also demonstrated with a dipole antenna, remotely powering LEDs to show how this concept can be applied in wireless power transfer.

II. Transmission Line RCN

A. Theoretical Development

Fig. 3 shows the basic single-stage TLRCN network section, loaded with identical resistive loads R_L, having an input port with driving point impedance Z_{in} that one desires to maintain near a specified value. The transmission line branches have lengths that can be expressed in terms of a base length plus and minus a delta length (or a base angle plus/minus a delta angle):

$$\begin{aligned} \ell_1 &= \ell_{\mathrm{base}} + \Delta\ell, \quad \ell_2 = \ell_{\mathrm{base}} - \Delta\ell \\ \theta_1 &= \theta_{\mathrm{base}} + \Delta\theta, \quad \theta_2 = \theta_{\mathrm{base}} - \Delta\theta \end{aligned} \tag{1}$$

While there are multiple possibilities for base lengths, we first consider a base length ℓ_{base} of $\lambda/4$ (a quarter wavelength at the operating frequency). In this case, the branch input

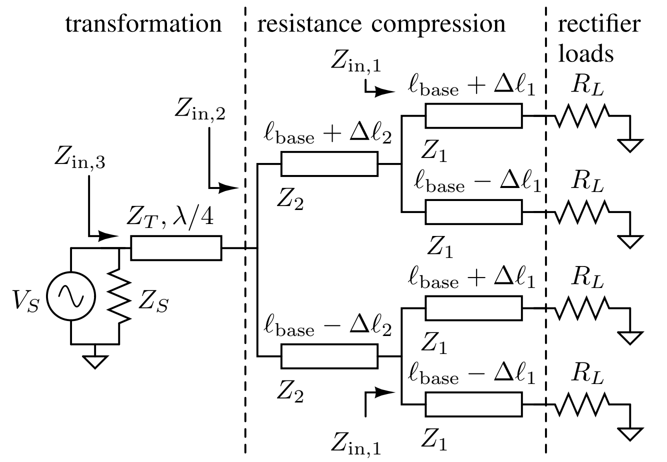

Fig. 2. Four-way TLRCN with quarter-wave impedance transformation stage. Each pair of transmission line lengths can be expressed in terms of a base line length plus and minus a delta length. The rectifiers are represented here as resistors with equal (but varying) value R_L.

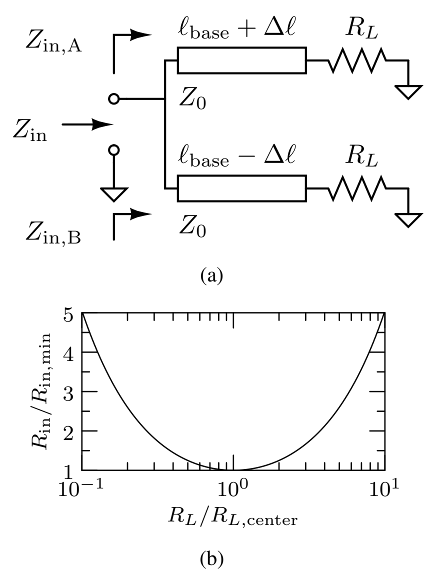

Fig. 3. Basic single-stage TLRCN and resistance compression behavior. (a) — topology, (b) — normalized input resistance vs. normalized load resistance for $Z_0 = R_{L,\text{center}}$, $\ell_{\text{base}} = \lambda/4$, and $\Delta\ell = \lambda/8$.

admittances at the operating frequency are:

$$\begin{aligned} Y_{\text{in,A}} &= \frac{1}{Z_0}\frac{Z_0 - jR_L\cot(\Delta\theta)}{R_L - jZ_0\cot(\Delta\theta)} \\ Y_{\text{in,B}} &= \frac{1}{Z_0}\frac{Z_0 + jR_L\cot(\Delta\theta)}{R_L + jZ_0\cot(\Delta\theta)} \end{aligned} \tag{2}$$

Because these admittances are complex conjugates, for identical load resistances the network will divide power entering the input port equally to both loads. In this case the input impedance seen at the input port at the operating frequency is resistive, and can be shown to be:

$$Z_{\text{in},\frac{\lambda}{4}} = \frac{|\cot(\Delta\theta)|}{2\left(1+\cot^2(\Delta\theta)\right)}\left(\frac{R_L}{|\cot(\Delta\theta)|} + \frac{Z_0^2}{\frac{R_L}{|\cot(\Delta\theta)|}}\right) \tag{3}$$

Alternatively, a base length of $\lambda/2$ can be chosen, in which case the input impedance of the single-stage TLRCN is:

$$Z_{\text{in},\frac{\lambda}{2}} = \frac{|\tan(\Delta\theta)|}{2\left(1+\tan^2(\Delta\theta)\right)}\left(\frac{R_L}{|\tan(\Delta\theta)|} + \frac{Z_0^2}{\frac{R_L}{|\tan(\Delta\theta)|}}\right) \tag{4}$$

Although a greater base length leads to longer total conduction paths in the combiner (and hence higher losses), a base length of $\lambda/2$ may be preferable in cases where the shorter ($\ell_{\text{base}} - \Delta\ell$) transmission line segment becomes impractically small. Furthermore, for either of these design options, operation will be the same with any additional multiple of $\lambda/2$ added to the base length, and this degree of freedom may be useful for controlling the input impedance at one or more harmonic frequencies. In the experimental demonstrations in this work, we use a $\lambda/4$ base length, as described in Section III-A below.

The characteristics in (3) and (4) clearly realize resistance compression, as the input impedance varies resistively over a small range when the load resistances vary together over a wide range. When a base length of $\lambda/4$ is chosen, for example, the network provides "balanced" compression for a range of load resistances having a geometric mean of $R_{L,\text{center}}$:

$$R_{L,\text{center}} = Z_0 \cdot |\cot(\Delta\theta)| \tag{5}$$

At this load resistance value $R_{L,\text{center}}$, the input resistance has minimum value $R_{\text{in,min}}$,

$$R_{\text{in,min}} = Z_0\frac{|cot(\Delta\theta)|}{1+\cot^2(\Delta\theta)} \tag{6}$$

and the ratio of the maximum to minimum input resistance is:

$$\frac{R_{\text{in,max}}}{R_{\text{in,min}}} = \frac{1}{2}\left(\sqrt{\frac{R_{L,\text{max}}}{R_{L,\text{min}}}} + \sqrt{\frac{R_{L,\text{min}}}{R_{L,\text{max}}}}\right) \tag{7}$$

For example, a 10:1 range of load resistance is compressed by a single-stage TLRCN to a 1.74:1 ratio in input resistance, and a 100:1 range in load resistance is compressed to only a 5.05:1 ratio of input resistance (Fig. 3b). These resistance compression characteristics are similar to those achieved with lumped-parameter (L,C) RCNs. Moreover, as shown in the appendix, the TLRCN also provides phase compression for matched reactive loads.

Other base lengths likewise result in equal power transfer to the two loads and resistance compression. For example, when a base length of $\ell_{\text{base}} = \lambda/2$ ($\theta_{\text{base}} = \pi$ radians) is chosen, the input resistance characteristics are the same as in (2)–(3) and (5)–(7) but with $\cot(\Delta\theta)$ replaced with $-\tan(\Delta\theta)$.

B. Design Procedures

In this section we present two approaches to TLRCN design, each providing particular benefits. In the first approach, a base length (here, $\lambda/4$) is chosen, and the delta length is chosen a priori to be $\Delta\ell = \lambda/8$ ($\Delta\theta = \pi/4$ radians). The characteristic impedance Z_0 is chosen equal to the geometric mean of the maximum and minimum load resistances of interest, $R_{L,\text{center}}$. As a result of this choice, the load resistances R_L vary geometrically about the transmission line characteristic impedance, which helps reduce the transmission line reflection and loss.

In cases where the resulting input resistance (range given by (6), (7)) is not at the desired value, an additional impedance transformation stage may be placed at the input of the TLRCN, for example by including an additional quarter-wave line at the input to the compression stage as in Fig 2. To accomplish this, the quarter-wave line is selected with a characteristic impedance that is the geometric mean of the desired input impedance $R_{\text{in,desired}}$, and an impedance approximating that presented by the remainder of the RCN system (e.g., $R_{\text{in,min}}$ or $(R_{\text{in,min}} + R_{\text{in,max}})/2$ as determined by (6), (7)).

The second design approach directly realizes both resistance compression and a desired specified input resistance using the topology in Fig. 3 by choosing both the differential length and the characteristic impedance of the transmission lines. As in the first approach, the center resistance $R_{L,\text{center}}$ is selected as the geometric mean of the maximum and minimum load resistances of interest, $R_{L,\max}$ and $R_{L,\min}$. One then defines a minimum input resistance $R_{\text{in,min}}$ to be realized by the resistance compression network. This minimum input resistance is selected based on the desired resistance $R_{\text{in,desired}}$ seen at the input of the TLRCN. For example, one may choose $R_{\text{in,min}} = R_{\text{in,desired}}$ (recognizing that the actual input resistance will be equal or greater than this desired value). Alternatively, one may choose the median value of the input resistance that occurs over the expected range of load resistances to match the desired input resistance. In this case, $R_{\text{in,min}}$ is selected as:

$$R_{\text{in,min}} = \frac{2 \cdot R_{\text{in,desired}}}{1 + \frac{1}{2}\sqrt{\frac{R_{L,\max}}{R_{L,\min}}} + \frac{1}{2}\sqrt{\frac{R_{L,\min}}{R_{L,\max}}}} \tag{8}$$

Based on selecting $R_{L,\text{center}}$ and $R_{\text{in,min}}$, the characteristic impedance Z_0 and value for $\Delta\theta$ can be directly chosen as follows (from (5) and (6), and for $\ell_{\text{base}} = \lambda/4$):

$$\cot(\Delta\theta) = \sqrt{\frac{R_{L,\text{center}}}{R_{\text{in,min}}} - 1} \tag{9}$$

$$Z_0 = \frac{R_{L,\text{center}}}{\sqrt{\frac{R_{L,\text{center}}}{R_{\text{in,min}}} - 1}} \tag{10}$$

An advantage of this design approach as compared to the first one is that, within practical limits, it may not require an additional impedance transformation stage and thus results in a more compact structure. However, as $R_{\text{in,min}}$ approaches $R_{L,\text{center}}$, the characteristic impedance of the transmission lines can grow impractically large. Furthermore, this approach applies only to applications where the desired input impedance to the TLRCN is below the range of load resistances, so that $R_{L,\text{center}}/R_{\text{in,min}} > 1$.

C. Multi-Way TLRCNs

One advantageous way to synthesize multi-way TLRCNs is by cascading single-level TLRCN networks in a tree structure (as seen in Fig. 2). If the first design methodology is chosen (in which $\Delta\theta$ is chosen a priori to be $\pi/4$), then the multi-stage TLRCN can be optimized in terms of minimizing the peak deviation from a median input resistance. We employ a technique akin to that described for lumped-parameter RCNs in [38], although in this case we design to maximize the compression for a particular range of load resistances, instead of maximizing the range of load resistances that gives a specified compression range. Starting from the TLRCN stage closest to the load (i.e., the rightmost stage in Fig. 2), each transmission line characteristic impedance is chosen based on the effective load it sees. For example, if as in the example in Fig. 4, the load varies over the range $[R/a, aR]$, suppose we want to design a four-way TLRCN that provides maximal resistance compression. When the first stage (closest to the load) is chosen to have $Z_1 = R$ (equal to the geometric mean of the load resistances) and $\Delta\ell = \lambda/8$, the input resistance $Z_{\text{in},1}$ (see Fig. 2) varies over the range $[0.5R, 0.5bR]$. The ratio of maximum to minimum input resistance b can be found from (7):

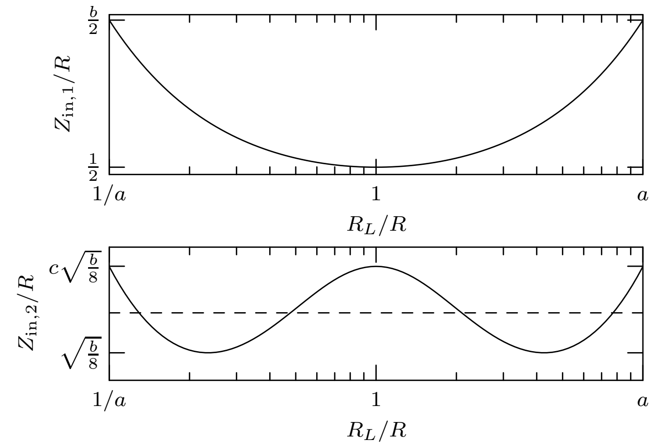

Fig. 4. Input resistance when multiple stages of TLRCNs are cascaded to create a four-way TLRCN as in Fig. 2, in this case with $Z_1 = R_{L,\text{center}}$, $Z_2 = \sqrt{\max(Z_{\text{in},1}) \cdot \min(Z_{\text{in},1})}$, $\Delta\ell_1 = \Delta\ell_2 = \lambda/8$, and the quarter-wave transmission line Z_T omitted.

$$b = \frac{1}{2}\left(\sqrt{\frac{aR}{R/a}} + \sqrt{\frac{R/a}{aR}}\right) = \frac{1}{2}\left(a + \frac{1}{a}\right) \tag{11}$$

The second TLRCN stage is then chosen to compress the $[0.5R, 0.5bR]$ range of load resistances seen at its terminals. The characteristic impedance of the lines is chosen to be the geometric mean of this range, $Z_2 = R\sqrt{b/2}$, and the input impedance $Z_{\text{in},2}$ ranges from a minimum $Z_2/2$, with ratio of maximum to minimum input resistance determined by (7).

This technique, with $\ell_{\text{base}} = \lambda/4$ and with an impedance transformation stage included at the input of the TLRCN, was used in the example design in this work. Alternatively, both the characteristic impedances and differential lengths of each stage can be optimized as in the second design approach, or a combination of approaches can be used.

III. Implementation and Measurements

A. TLRCN Design

For our example implementation, we assume that the resistive loads will vary over a 18–170 Ω range, corresponding to

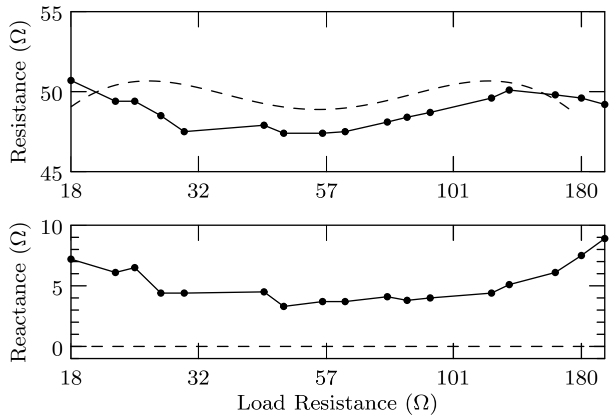

Fig. 5. Theoretical (dashed) and measured (solid) input resistance and reactance to the two-stage TLRCN when it is terminated with resistive loads. The phase of the input impedance remains within about 4 degrees over the entire 18–170 Ω operating range.

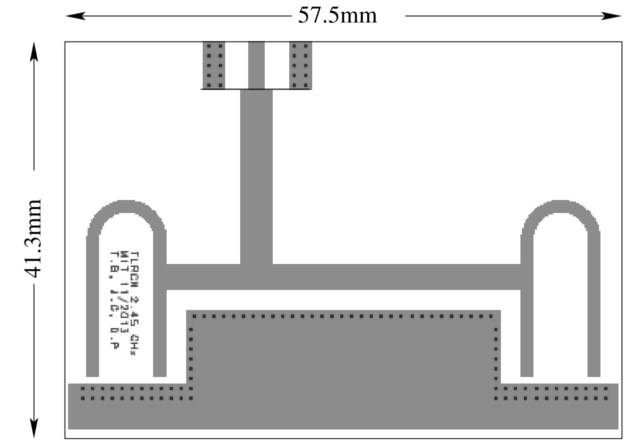

Fig. 6. TLRCN test structure layout, used to characterize the network's performance using resistive terminations. The microstrip design was implemented on a 30-mil Rogers 4350 substrate with a ground plane as the other side of the board. Parasitics including via inductance and resistor package parasitics were characterized and compensated for with shunt capacitors at the loads, so that the load impedance presented to the TLRCN at its reference plane was purely resistive.

four tuned rectifiers acting as variable and approximately resistive loads. We choose a base transmission line length $\ell_{\text{base}} = \lambda/4$ and $\Delta\ell = \lambda/8$, and use the four-way TLRCN with quarter-wave impedance transformation stage shown in Fig. 2, following the design procedure outlined in Section II-C. In the first compression stage, we choose $Z_1 = \sqrt{18 \cdot 170} = 55$ Ω, so that this stage compresses the resistances presented by the loads into a range of 27.5 Ω $\leq Z_{\text{in},1} \leq$ 46.7 Ω. This resistance range acts as the load for the second stage of compression. Again following the first design approach from Section II-B, the characteristic impedance for the second stage is chosen as $Z_2 = \sqrt{27.5 \cdot 46.7} = 36$ Ω (and $\Delta\ell = \lambda/8$). The compressed input resistance $Z_{\text{in},3}$ (see Fig. 2) varies over a 18–18.55 Ω range. The transformation stage, comprising a quarter-wave line with characteristic impedance $Z_T = 30.2$ Ω, transforms this impedance into the desired overall input impedance of approximately 50 Ω. The calculated input impedance when R_L varies over a 18–170 Ω range is shown in Fig. 5 (dashed lines).

The layout of the TLRCN test structure (to be resistively terminated) is shown in Fig. 6. Transmission line dimensions were initially found using [39] and were input into Agilent ADS for simulation. The microstrip lengths were adjusted to account for the radiusing (used to produce a compact design) based on equations for effective transmission line lengths in [40]. To account for the effective electrical length of the three T junctions, it was assumed that the nonidealities of the junction are symmetric for the lengths forming the top bar of each "T," so those lengths were trimmed equally in simulation. In the iterative design process, the S-parameters of the extracted layout were compared to the ideal values, and length adjustments were performed to produce a close match.

The four-way TLRCN was fabricated on a 30-mil thick Rogers RO4350 substrate and characterized at 2.45 GHz by resistively terminating its four load ports over the range 18-200 Ω. For these measurements, the parasitic inductance (due to vias, resistor package parasitics, etc.) of each resistor value was measured and compensated for using parallel capacitors, so that the impedance presented at the reference planes of the TLRCN loads were purely resistive. The measured input impedance is shown in Fig. 5. The resistance compression effect is evident — when the load is varied over a 11:1 range, the input resistance varies over only a 1.07:1 range. For comparison, a single-stage TLRCN designed to operate over the same load resistance range would compress this impedance to only a (calculated) 1.7:1 range.

B. *Class-E Resonant Rectifier*

For this application it is desirable to design the rectifier to have a resistive input impedance over the desired range of input power levels (although some reactance can be tolerated as indicated in the appendix). We therefore follow the methodology in [20] to design a class-E rectifier with near-resistive input impedance over a wide range of power levels at 2.45 GHz. The rectifier topology, including trim components used in the prototype system to counteract the parasitic effects of layout, device packaging, and passive components, is shown in Fig. 7. Component values are shown in Table I. In keeping with the high-power wireless power transfer applications of interest here, we select the Avago HBAT540B diode for its high power-handling capability (among devices capable of operating at GHz frequencies). The inductor $L_r = 2.2$ nH is chosen to resonate with the diode's parasitic shunt capacitance, C_D, following the methodology in [20] and accounting for package parasitics. A 9-V zener diode acts as the rectifier load. This topology was simulated in Agilent ADS (omitting trim components) using a complete package model for the diode, and found to have an input impedance varying from 20 – 180 Ω over a 100 mW – 1W operating range with only 12° maximum input impedance phase at 2.45 GHz.

The fabricated rectifier was first characterized individually by using a through power meter (Rohde&Schwarz NRT-Z44) to record total input power from the driving power amplifier,

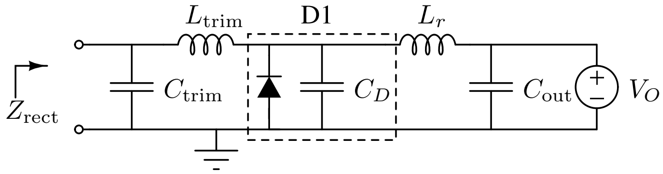

Fig. 7. Schematic of the resonant class-E rectifier used as a load in the system prototype.

TABLE I
CLASS-E RECTIFIER COMPONENT VALUES

Component	Value	Mfr. Part #	Mfr.
D_1	–	HBAT540B	Avago
L_r	2.2 nH	0402HP-2N2X	CoilCraft
L_{trim}	2.7 nH	0402HP-2N7X	
C_{trim}	0.7 pF	600F 0R7JT	ATC
	27 pF ||	600L 270JT	
C_{out}	10 pF ||	MC12FA241J-F	CDE
	100 pF	MC08CA100D-F	

as well as the the SWR resulting from power-level-dependent impedance mismatch at the rectifier input. With the trim components omitted, the rectifier had high measured SWR when driven at the power level expected to produce a 50-Ω input impedance. The overall input impedance was determined to be capacitive, which is explained by the operation of the LC tank below its resonant frequency. A trim inductor $L_{\text{trim}} = 2.7$ nH was included to offset this capacitance, and experimentally selected to minimize SWR when the input power was at the value expected to produce a 50-Ω input resistance. Due to a limited range of available inductor values (and physical layout constraints), a shunt capacitor $C_{\text{trim}} = 0.7$ pF was included and found experimentally to minimize SWR at 27 dBm input power. This LC network thus trims out the capacitive component of the input impedance owing to the rectifier's inherent input characteristics and effects of the inductive via connections to ground. The resulting efficiency and SWR measurements of a single rectifier when $V_O = 9$ V are shown in Fig. 9 (dashed lines). Despite the trimming of input reactance, the rectifier has higher SWR than expected from resistive load mismatch alone, and thus must have some uncompensated input reactance. It can be seen that the peak rectifier efficiency of $\sim 70\%$ is extremely good (for 2.45 GHz), but that efficiency of capturing incident energy tends to fall off significantly at lower incident power levels, in large part owing to the impedance mismatch caused by the rectifier impedance changing with power (as evidenced by the high SWR). Nonetheless, the TLRCN is able to compress this impedance range to impedances near 50 Ω, as demonstrated below.

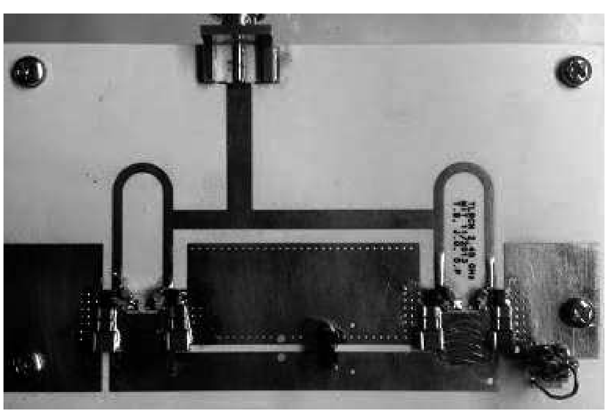

Fig. 8. Photograph of the prototype 2.45-GHz TLRCN and rectifiers.

C. System Measurements

In order to demonstrate the benefits of this approach in a rectenna the TLRCN was terminated with four rectifiers as shown in Fig. 8 and characterized in terms of efficiency and SWR over a 0.26 W to 4.16 W range. For this proof-of-concept characterization, the input was driven directly by an RF source (without antenna). Efficiency is therefore characterized including mismatch loss and rectifier efficiency, but does not include any characterization of antenna efficiency.

Measured results are shown on an input power per rectifier basis in Fig. 9 (solid lines) in order to facilitate a direct comparison. Including the TLRCN between the rectifier loads and the rf source dramatically improves the impedance match over a wide input power range, thus improving both overall efficiency and dynamic range. Despite the high variation in rectifier load impedance, the input SWR remains under 1.4 over the entire 11 dB input power range, and under 1.1 over the upper 7.7 dB of the measurement. The system has rf-to-dc efficiency above 50% over a 10.1-dB range of input powers, with a peak efficiency of 70%. Furthermore, losses associated with including the TLRCN network between the rf source and rectifiers are offset by the improved impedance match, so that efficiency is not degraded at incident power levels where the unmatched rectifier impedance is closest to 50 Ω. These measurements demonstrate the excellent rf-to-dc performance that is achievable with TLRCNs, in terms of efficiency, maintaining a desired load match across a wide power range, and simplicity of implementation in microstrip form.

The reduction in microwave-to-dc efficiency at the lower end of the power range is related to the resonant currents between the rectifier capacitor and resonant inductor. Simulations of the topology in Fig. 7 confirm that the magnitude of these resonant currents are relatively constant over the 10:1 power range. Because the output voltage is also fixed, but output power is reduced, overall efficiency is reduced. This characteristic could be improved by including an additional MPPT power converter to track the optimal output voltage, but at the cost of additional complexity, size and bandwidth limitations. The high bandwidth and lack of need for a subsequent controlled converter stage, along with the distribution of power among multiple rectifying devices, are advantages of the TLRCN-based design.

In order to illustrate this approach in a true wireless power system, we performed a simple experiment of lighting four

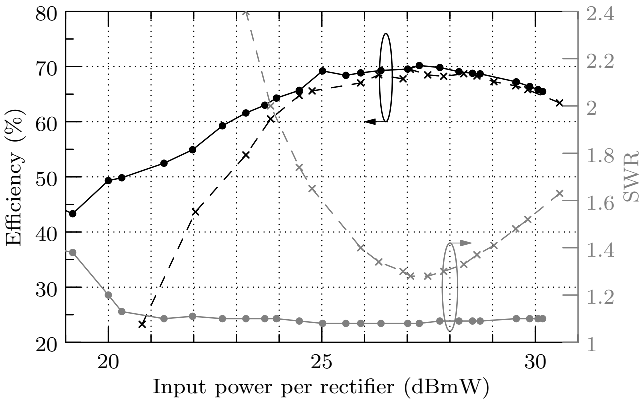

Fig. 9. Efficiency of a single rectifier (dashed), and four rectifiers plus the TLRCN (solid), including losses due to impedance mismatch. The measured standing wave ratio (SWR) is also shown. Including the TLRCN substantially improves the impedance match over the entire input power range.

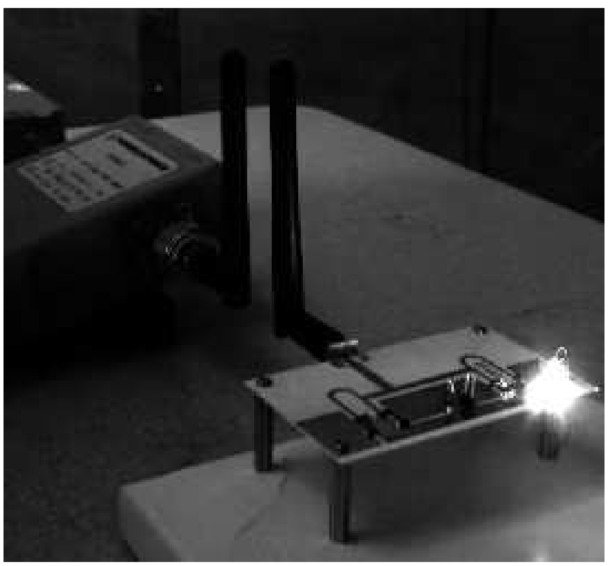

Fig. 10. Photograph of a string of four LEDs being wirelessly powered by the TLRCN/rectifier system.

series-connected LEDs (total voltage drop approximately 9 V) wirelessly using dipole antennas. A photograph of this demonstration is shown in Fig. 10.

IV. Conclusion

This paper introduces the use of multi-stage TLRCNs for rf rectification. The approach has several advantages over a matching network designed for a single load impedance, including minimizing the effective input impedance variation across power level and distributing the input power among multiple devices. We introduce two design methods for TLRCN systems (applicable to both single- and multi-stage designs), to achieve a desired input resistance. We demonstrate a multi-stage TLRCN with a design example for resistive load variation over a 18–170 Ω range and operating at 2.45 GHz. When loaded with this range of real impedances at its four load ports, this network achieves an input resistance variation

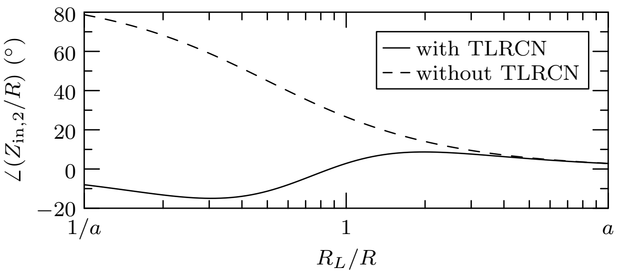

Fig. 11. An additional advantage of the TLRCN is that is provides phase compression when its multiple loads have some (equal) reactive component. This example is calculated for a single-stage TLRCN with $Z_0 = 1$, $\ell = \lambda/4$, $\Delta\ell = \lambda/8$, and a load with resistive component varying over the range $[R/a, aR]$ in series with a fixed series reactance of $0.5R$.

of only 1.07:1. Combined with class-E resonant rectifiers, which present a theoretically near-resistive range of input impedances, the system has SWR < 1.1 over 7.7-dB power range and < 1.4 over a 16-dB power range. The demonstrated 4-W, 2.45-GHz TLRCN-based rectifier system achieves a peak rf-to-dc energy capture efficiency of 70%, with an efficiency of $> 50\%$ maintained for more than a 10-dB power range.

Appendix

Practical rectifier implementations, particularly ones at microwave frequencies, will not necessarily provide the ideally resistive input impedance assumed in Section II. In this appendix, we investigate the effects of replacing the load resistors in Fig. 3(a) with complex impedances.

If the reactive components are matched among the multiple rectifier loads (for example, due to fixed parasitic elements of the layout, device packaging, etc.), the TLRCN also provides phase compression of the input impedance. That is, the input impedance the the TLRCN will appear more resistive than the loads. An example of this behavior is shown in Fig. 11, in which the phase of the TLRCN input impedance is calculated for a single-stage TLRCN with $\ell = \lambda/4$ and $\Delta\ell = \lambda/8$. In this example, a fixed normalized reactance of $+j0.5$ is included in series with the resistive component (which varies over the range $[R/a, aR]$). Without the TLRCN, the phase of the input impedance would vary over a 75-degree range, but this is compressed to 24 degrees by the TLRCN. As with resistive load compression, multiple TLRCN stages can be cascaded to improve the compression.

In general, if the load impedances are complex then at the operating frequency the load impedances can be expressed as:

$$Z_L = R_L + jX_L = |Z_L|\angle\alpha \tag{12}$$

When this impedance is substituted for R_L in the equation for effective input impedance to the TLRCN with quarter-wave base length (3), the input impedance can be shown to be:

$$Z_{\mathrm{in},\frac{\lambda}{4},\mathrm{Z_L}} = \left(\frac{1}{2\left(1+\cot^2(\Delta\theta)\right)}\right)$$
$$\left(\frac{(R_L(R_L^2 + X_L^2 + Z_0^2\cot^2(\Delta\theta))}{R_L^2 + X_L^2}\right.$$

$$+ \frac{jX_L(R_L^2 + X_L^2 - Z_0 \cot^2(\Delta\theta))}{R_L^2 + X_L^2}\Bigg) \tag{13}$$

If this input impedance is expressed in terms of magnitude and phase as $Z_{\text{in},\frac{\lambda}{4},\text{Z}_\text{L}} = |Z_{\text{in}}|\angle\beta$, then the phase of the input impedance is:

$$\tan\beta = \frac{X_L}{R_L}\left(\frac{R_L^2 + X_L^2 - Z_0^2\cot^2(\Delta\theta)}{R_L^2 + X_L^2 + Z_0^2\cot(\Delta\theta)}\right) \tag{14}$$

$$\tan\beta = \tan\alpha\left(\frac{|Z_L|^2 - Z_0\cot^2(\Delta\theta)}{|Z_L|^2 + Z_0^2\cot^2(\Delta\theta)}\right) \tag{15}$$

Recognizing that the term in the parentheses in (15) will always have magnitude less than one (for either inductive or capacitive load impedance X_L), it follows that $|\beta| < |\alpha|$. A similar result is found in the case of a half-wavelength base length, in which case $\cot(\Delta\theta)$ is replaced with $-\tan(\Delta\theta)$. From (15), it can be seen that for the effective input impedance to be purely resistive (independent of the phase of the load impedance, α), the network should be designed such that $Z_0\cot(\Delta\theta) = |Z_L|$.

References

[1] P. Godoy, D. Perreault, and J. Dawson, "Outphasing energy recovery amplifier with resistance compression for improved efficiency," *IEEE Trans. Microw. Theory Tech.*, vol. 57, no. 12, pp. 2895–2906, 2009.

[2] W. Nitz, W. Bowman, F. Dickens, F. Magalhaes, W. Strauss, W. B. Suiter, and N. Ziesse, "A new family of resonant rectifier circuits for high frequency dc-dc converter applications," *Appl. Power Electron. Conf. and Expo.*, pp. 12–22, 1988.

[3] J. Rivas, J. Shafran, R. Wahby, and D. Perreault, "New architectures for radio-frequency dc-dc power conversion," *IEEE Trans. Power Electron.*, vol. 21, no. 2, pp. 380–393, March 2006.

[4] J. Rivas, D. Jackson, O. Leitermann, A. Sagneri, Y. Han, and D. Perreault, "Design considerations for radio-frequency dc-dc converters," *IEEE Power Electron. Specialists Conf.*, pp. 2287–2297, June 2006.

[5] J. McSpadden, F. Little, M. Duke, and A. Ignatiev, "An in-space wireless energy transmission experiment," in *Energy Conversion Engineering Conference, 1996. IECEC 96., Proceedings of the 31st Intersociety*, vol. 1, Aug 1996, pp. 468–473 vol.1.

[6] C. Bergsrud, S. Noghanian, J. Straub, D. Whalen, and R. Fevig, "Orbit-to-ground wireless power transfer test mission," in *Aerospace Conference, 2013 IEEE*, March 2013, pp. 1–11.

[7] K. Tanaka, T. Fujita, S. Yamaguchi, S. Hamada, K. Miyashiro, and S. Sasaki, "System consideration of solar power satellite using functional models," in *Microwave Workshop Series on Innovative Wireless Power Transmission: Technologies, Systems, and Applications (IMWS), 2011 IEEE MTT-S International*, May 2011, pp. 195–198.

[8] W. C. Brown and E. Eves, "Beamed microwave power transmission and its application to space," *Microwave Theory and Techniques, IEEE Transactions on*, vol. 40, no. 6, pp. 1239–1250, Jun 1992.

[9] E. Okress, W. Brown, T. Moreno, G. Goubau, N. Heenan, and R. George, "Microwave power engineering," *Spectrum, IEEE*, vol. 1, no. 10, pp. 76–76, Oct 1964.

[10] J. Bernhard, K. Hietpas, E. George, D. Kuchima, and H. Reis, "An interdisciplinary effort to develop a wireless embedded sensor system to monitor and assess corrosion in the tendons of prestressed concrete girders," in *IEEE Trans. Wireless Commun.*, 2003, pp. 241–243.

[11] E. Falkenstein, M. Roberg, and Z. Popovic, "Low-power wireless power delivery," *IEEE Trans. Microw. Theory Tech.*, vol. 60, no. 7, pp. 2277–2286, 2012.

[12] J. McSpadden, T. Yoo, and K. Chang, "Theoretical and experimental investigation of a rectenna element for microwave power transmission," *IEEE Trans. Microw. Theory and Tech*, vol. 40, no. 12, pp. 2359–2366, 1992.

[13] G. Andia Vera, A. Georgiadis, A. Collado, and S. Via, "Design of a 2.45 GHz rectenna for electromagnetic (EM) energy scavenging," in *Proc. IEEE Radio Wireless Symp.*, 2010, pp. 61–64.

[14] J. Hagerty, F. Helmbrecht, W. McCalpin, R. Zane, and Z. Popovic, "Recycling ambient microwave energy with broad-band rectenna arrays," *IEEE Trans. Microw. Theory Tech.*, vol. 52, no. 3, pp. 1014–1024, 2004.

[15] A. Sample and J. Smith, "Experimental results with two wireless power transfer systems," in *Proc. IEEE Radio Wireless Symp*, 2009, pp. 16–18.

[16] W. C. Brown, "The history of power transmission by radio waves," *IEEE Trans. Microw. Theory Tech.*, vol. 32, no. 9, pp. 1230–1242, 1984.

[17] S. Keyrouz, H. Visser, and A. Tijhuis, "Rectifier analysis for radio frequency energy harvesting and power transport," in *IEEE European Microw. Conf.*, 2012, pp. 428–431.

[18] Y. Han, O. Leitermann, D. A. Jackson, J. M. Rivas, and D. J. Perreault, "Resistance compression networks for radio-frequency power conversion," *IEEE Trans. Power Electron.*, vol. 22, no. 1, pp. 41–53, Jan. 2007.

[19] H. Visser, "Aspects of far-field rf energy transport," in *IEEE European Microw. Conf.*, 2012, pp. 317–320.

[20] J. Santiago-Gonzalez, K. Afridi, and D. Perreault, "Design of resistive-input class E resonant rectifiers for variable-power operation," in *IEEE Workshop on Control and Modeling for Power Electron.*, 2013, pp. 1–6.

[21] M. Del Prete, A. Costanzo, D. Masottii, and A. Romani, "An alternative rectenna design approach for wirelessly powered energy autonomous systems," in *IEEE MTT-S Int. Microw. Symp.*, 2013, pp. 1–4.

[22] A. Dolgov, R. Zane, and Z. Popovic, "Power management system for online low power rf energy harvesting optimization," *Circuits and Systems I: Regular Papers, IEEE Transactions on*, vol. 57, no. 7, pp. 1802–1811, July 2010.

[23] Y. Huang, N. Shinohara, and T. Mitani, "A study on low power rectenna using dc-dc converter to track maximum power point," in *Microwave Conference Proceedings (APMC), 2013 Asia-Pacific*, Nov 2013, pp. 83–85.

[24] M. Dini, M. Filippi, A. Costanzo, A. Romani, M. Tartagni, M. Del Prete, and D. Masotti, "A fully-autonomous integrated rf energy harvesting system for wearable applications," in *Microwave Conference (EuMC), 2013 European*, Oct 2013, pp. 987–990.

[25] V. Marian, B. Allard, C. Vollaire, and J. Verdier, "Strategy for microwave energy harvesting from ambient field or a feeding source," *Power Electronics, IEEE Transactions on*, vol. 27, no. 11, pp. 4481–4491, Nov 2012.

[26] R. Dickinson, "Power in the sky: Requirements for microwave wireless power beamers for powering high-altitude platforms," *Microwave Magazine, IEEE*, vol. 14, no. 2, pp. 36–47, March 2013.

[27] J. Gavan and S. Tapuchi, "The potential of high altitude platforms (haps) for low interference and broadband radio services," in *Environmental Electromagnetics, 2009. CEEM 2009. 5th Asia-Pacific Conference on*, Sept 2009, pp. 17–25.

[28] T. Tozer and D. Grace, "High-altitude platforms for wireless communications," *Electronics Communication Engineering Journal*, vol. 13, no. 3, pp. 127–137, Jun 2001.

[29] A. Mohammed, A. Mehmood, F.-N. Pavlidou, and M. Mohorcic, "The role of high-altitude platforms (haps) in the global wireless connectivity," *Proceedings of the IEEE*, vol. 99, no. 11, pp. 1939–1953, Nov 2011.

[30] W. Inam, K. Afridi, and D. Perreault, "High efficiency resonant dc/dc converter utilizing a resistance compression network," in *IEEE Trans. Power Electron.*, 2014 (early access).

[31] T. W. Barton, J. L. Dawson, and D. J. Perreault, "Experimental validation of a four-way outphasing combiner for microwave power amplification," *IEEE Microw. Wireless Compon. Lett.*, vol. 23, no. 1, pp. 28–30, Jan. 2013.

[32] T. W. Barton, J. L. Dawson, and D. J. Perreault, "Four-way lossless outphasing and power combining with hybrid microstrip/discrete combiner for microwave power amplification," in *IEEE MTT-S Int. Microw. Symp. Dig.*, June 2013, pp. 1–4.

[33] D. J. Perreault and J. L. Dawson, "RF energy recovery system," U.S. Patent Application US 2013/0 343 106 A1, Dec. 26, 2013.

[34] D. J. Perreault, "Transmission-line resistance compression networks and related techniques," U.S. Patent Application US 2013/0 343 107 A1, Dec. 26, 2013.

[35] J. Xu and D. Ricketts, "An efficient, watt-level microwave rectifier using an impedance compression network (ICN) with applications in outphasing energy recovery systems," *IEEE Microw. Wireless Compon. Lett.*, vol. 23, no. 10, pp. 542–544, 2013.

[36] J. Xu, W. Tai, and D. Ricketts, "A transmission line based resistance compression network (TRCN) for microwave applications," *IEEE MTT-S Int. Micro. Symp. Dig.*, pp. 1–4, June 2013.

[37] T. Barton, J. Gordonson, and D. Perreault, "Transmission line resistance compression networks for microwave rectifiers," *IEEE MTT-S Int. Microw. Symp. Dig.*, pp. 1–4, June 2014 (to appear).

[38] D. Perreault, "A new power combining and outphasing modulation system for high-efficiency power amplification," *IEEE Trans. Circuits Syst. I: Reg. Papers*, vol. 58, no. 8, pp. 1713–1726, Feb. 2011.
[39] Microstrip Analysis/Synthesis Calculator, Accessed July 2013. [Online]. Available: http://wcalc.sourceforge.net/cgi-bin/microstrip.cgi
[40] G. Kompa, *Practical Microstrip Design and Applications*. Norwood, MA: Artech House, 2005.

Taylor W. Barton (S'07, M'12) received the Sc.D degree from the Massachusetts Institute of Technology (Cambridge, MA) in 2012 for her research in energy-efficient power amplifiers for wireless communications. She also holds B.S., M.Eng., and E.E. degrees from MIT's department of Electrical Engineering and Computer Science. In 2007 she joined the MIT Microsystems Technology Laboratory where she has also been a Postdoctoral Associate since 2013. Before starting as a post-doc, she was a visiting lecturer at MIT lecturing solid state circuits. Her research interests include high-efficiency RF and analog circuit design, and classical control theory.

Joshua M. Gordonson received the B.S. degree in Electrical Science and Engineering from the Massachusetts Institute of Technology, Cambridge, MA, in 2012, where he continues to pursue the M.Eng. degree. His research interests include power electronics, analog and RF circuit design, and design for educational electronics.

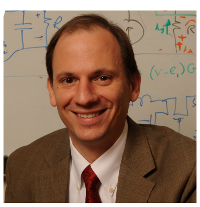

David J. Perreault (S91, M97, SM 06, F13) received the B.S. degree from Boston University, Boston, MA, and the S.M. and Ph.D. degrees from the Massachusetts Institute of Technology, Cambridge, MA. In 1997 he joined the MIT Laboratory for Electromagnetic and Electronic Systems as a Postdoctoral Associate, and became a Research Scientist in the laboratory in 1999. In 2001, he joined the MIT Department of Electrical Engineering and Computer Science, where he is presently Professor and Associate Department Head. His research interests include design, manufacturing, and control techniques for power electronic systems and components, and in their use in a wide range of applications. He also consults widely in industry, and is co-founder of Eta Devices, a startup company focusing on high-efficiency RF power amplifiers. Dr. Perreault received the Richard M. Bass Outstanding Young Power Electronics Engineer Award from the IEEE Power Electronics Society, an ONR Young Investigator Award, and the SAE Ralph R. Teetor Educational Award, and is co-author of six IEEE prize papers.